UNIVERSITÄT BONN

K223: Nuclear γ–γ Angular Correlation

Advanced Laboratory Course

Contents

Introduction

In general, the radiation from electromagnetic multipoles is anisotropic. This is also valid for the radiative decays of nuclei. However, at the lab one observes an isotropic distribution because the angle of emission depends on the orientation of the nuclear spin and in nature these spins are oriented statistically. By using a cascade of decays of ^{60}Co we want to investigate the angular correlation between the two emitted γ-rays and confirm the prominent $4 \to 2 \to 0$ spin cascade in the daughter nucleus ^{60}Ni by comparing the measured data to the theoretically predicted directional correlation function.
The first thing we have to do is to calibrate the detectors and to set up the electronics to be able to identify the true coincidences. After that we can perform the main measurement of the coincident rates at various angles ϑ. The obtained data allow to test the theoretical models and to find the multipole transitions of the nucleus.

1. Theory

1.1. γ–γ cascades

The theoretical derivations here follow [2].
As derived in [2], the angular distribution of a $I_i \to I \to I_f$ cascade with differences L_1, L_2 in angular momentum can be written as

$$W(\theta) = 1 + A_{22}P_2(\cos\theta) + \cdots + A_{k_{max}k_{max}}P_{k_{max}}(\cos\theta)$$

where θ is the angle between the two γ-rays, P_i are the i-th Legendre Polynomials and $k_{max} = \min(2I, 2L_1, 2L_2)$. The coefficients A_{kk} are also given in [2].
We want to confirm that ^{60}Ni decays in a $4 \to 2 \to 0$ cascade, so try to fit the function

$$W(\theta) = 1 + A_{22}P_2(\cos\theta) + A_{44}P_4(\cos\theta) \tag{1.1}$$

to our data.
Because the spins in nuclei are oriented randomly, usually the observed angular distribution of the radiation emitted in decays is isotropic. The angular distribution $W(\theta)$ is only visible if nuclei with a preferred axis are selected.
Such a selection is possible if there is a cascade of two rays, in this case γ-rays, by taking a coincidence measurement with a fixed detector and a mobile detector at a relative angle ϑ to the

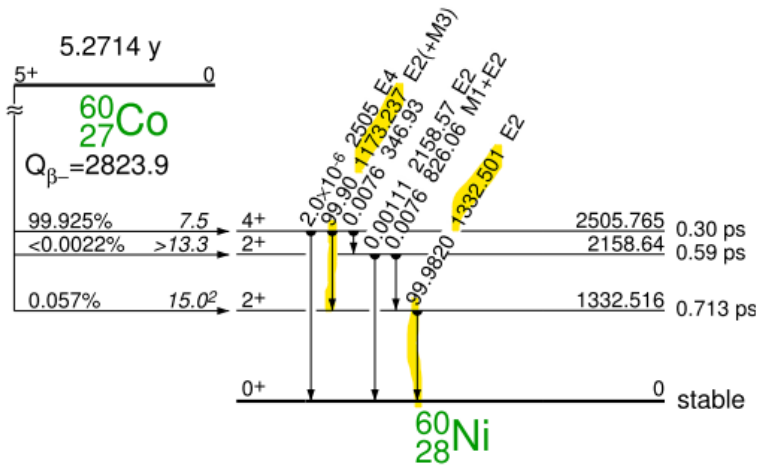

Figure 1.1.: Decay scheme of ^{60}Co. The transitions of the 4-2-0 spin cascade are marked. (adapted from [1])

axis of the fixed detector, see Fig. 1.2. In this manner the direction of the first ray is fixed and the directional correlation of the second ray can be determined. But one needs to consider that the angle θ between the two rays may be slightly different from ϑ because the detectors are covering a finite solid angle.
This leads to the fact that the values for A_{22}^{theo} and A_{44}^{theo} known from theory do not match the experimental results. In order to sort this problem out, we have to introduce correction factors Q_k:

$$A_{kk}^{\text{theo}} = A_{kk}^{\text{exp}} / Q_k^2$$

These factors depend on the distance between the source and the detector and the energy of the transition. A table of the factors, extracted from [2], can be found in Fig.A.1.

1.2. Detectors

The setup we are using to measure the correlation is shown in Fig. 1.2. The description of the detectors and the electronics is based on [3].

Scintillator The γ-rays are detected with scintillators, in this case NaI(Tl)-scintillators. The NaI(Tl) crystal absorbs the energy of the incoming γ-rays. The energy is then reemitted in the visible spectrum, and the reemitted energy is proportional to the energy of the original pulse.

Photomultiplier The photons produced by the scintillator are guided into a photomultiplier, where they liberate electrons from a photocathode via the photoelectric effect. These electrons are then accelerated towards further dynodes, where they again liberate more electrons. The number of electrons that are produced is proportional to the energy of the incoming photon, so the energy of the γ-rays is proportionally translated into an electric current.

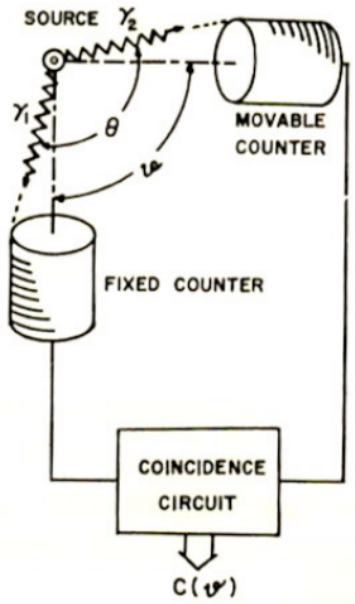

Figure 1.2.: The setup used to measure the angular correlation [2]

Expected Spectrum The expected energy spectrum of the radiation emitted from the source consists of the characteristic photopeaks by the transitions in the nuclei and the spectra of scattering effects. At very low energies one observes a peak of back-scattered photons from the matter around the source. This peak is followed by the Compton continuum that ends with the so-called Compton edge right before the photopeaks. It is created by photons that were scattered in the detector. The high count rate at the Compton edge is due to 180°-scattering. If the photons carry energies that allow the creation of e^-e^+-pairs, there are two additional peaks in the spectrum: the single- and the double-escape peak. Since the e^+ will annihilate in the detector material, one or both of the created photons from the annihilation may be lost. Therefore, these escape-peaks are situated at $E - 511\text{keV}$ or $E - 1022\text{keV}$ with E denoting the energy at the photopeak.

1.3. Electronics

The overall electronic setup we are building is pictured in Fig. 1.3. The signals from the detectors are split into a fast signal, that is used mainly for timing information, and a slow signal, that is mainly used for pulse height/energy information. In addition to the fast slow coincidence setup, which leads to a counter for the coincident signals, both slow branches are also fed into counters to determine the rates in each of the detectors.
All modules we use to further analyse the signals follow the NIM-standard.

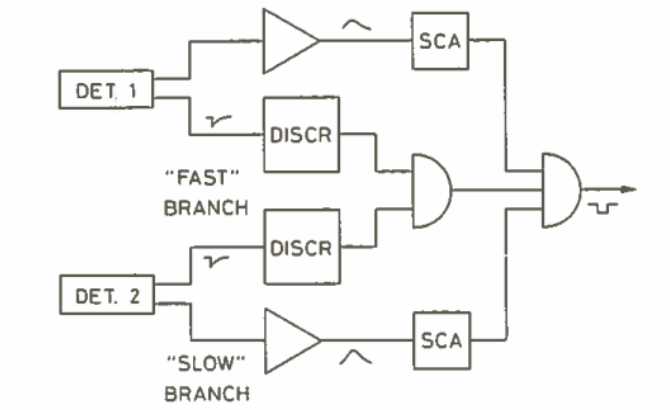

Figure 1.3.: The setup used to determine if two signals are coincident [3]

1.3.1. Slow Branch

In the slow branch, we are interested in detecting signals that were emitted in the transition, corresponding to the photopeaks of the spectrum. We expect the spectrum to have several other contributions, caused for example by backscattering, such as the Compton-edge.

Amplifier To be able to set the window more exactly we first amplify the signal, so the highest energy corresponds to about 8V, leaving a bit of headroom to the uppermost possible value of 10V.

Single Channel Analyser The Single Channel Analyser (SCA) allows us to only select signals in a fixed energy range. Our goal is to set this range so that only signals from the photopeaks, and no other contributions, lead to a signal in the counters. To set this window we first sweep across the entire available region of energies to get a spectrum of the energy measured in the detectors. This allows us to identify which scale setting corresponds to the photopeaks, and choosing appropriate lower and upper bounds to exclude unwanted signals. The signals from the SCAs are fed into counters, and also into the universal coincidence where they are compared to the signals from the fast branch.

1.3.2. Fast Branch

We are interested in the fast branch because it can help us to determine if two signals arrive at the same time. Theoretically, we would expect the second signal to be emitted later than the first, the delay should be about the lifetime of the unstable state. However, its lifetime is about three orders of magnitude lower than the resolving time of the electronics, so we can neglect this difference.

Constant Fraction Discriminator The signals in the fast circuits contain electric noise. A Constant Fraction Discriminator (CFD) allows us to set a minimum energy a signal must possess

without losing timing information. The CFD always triggers when the signal has reached a certain percentage of its maximum amplitude. This is done by inverting and delaying a part of the signal and adding this to the original signal. We look at the counts we get for several values of the threshold, also without the source in front of the detectors, so we can determine which part of the count rate is unwanted noise. Then we can set the threshold such that most of the noise is filtered out, but all of the information from the source is still present.

Coincidence in the Fast Circuit We want to get a signal when both detectors register a γ-ray at the same time. The time is distorted by the cables used to connect the detectors. To be able to circumvent this effect we introduce a fixed delay in one circuit and a variable delay in the other. We set the variable delay such that both signals truly arrive at the same time.
To set this up, we assume our source gives two signals at exactly the same time, and measure the counts for several values of the variable delay. We then choose the variable delay such that the count is maximized. To be able to align this signal with the signal from the slow circuits we feed it through an additional Gate and Delay.

Coincidence between Fast and Slow Circuit At the end we want to determine how many signals arrive with the right energy and at the same time. For this we set up a Universal Coincidence (UC) with three inputs, the coincidence from the fast circuits and the signals from both slow circuits. To align these signals we first put them on an oscilloscope and trigger from the fast circuit to ensure we have the signals at the same time. Then we align each of the signals from the slow circuit by adjusting the delay in the SCA to make sure they arrive at the same time at the universal coincidence. We can also adjust the delay from the gate at the fast coincidence. The output from the UC is then put into a counter.

1.4. Preparatory tasks

Here we give our answers to the preparatory questions asked in the script for the experiment [1]. This section contains some information that was already given previously, but we want to present it in the form asked by the script as well.

1.4.1. Which distances to choose?

- The count rate decreases as $1/r^2$, since according to [2]: $N \propto \Omega \propto \frac{A}{4\pi r^2}$ with A the detector surface and r the distance between source and detector.
- According to [2], the true and accidental coincidence rates are both proportional to the individual count rates in the detectors, so $C \propto \Omega_1\Omega_2 \propto \frac{A^2}{r_1^2 r_1^2}$. So overall the coincidence decreases like $\frac{1}{r^4}$.
- The expected coincidence rate is calculated for infinitesimally small solid angles, so in the real measurements, we have to introduce corrections factors for finite solid angles. We do not measure A_{kk}, but $A_{kk}^{\exp} = A_{kk}Q_k^2$. The correction factors Q_k are given for example in [2].

- We are not measuring the coefficients A_{kk} themselves, but $A_{kk}Q_k^2$. Gaussian error propagation leads us to conclude that correcting for these factors reduces the value for A_{kk} and its error by the same amount. However, $Q_2 > Q_4$, so after the correction the value for A_{22} will be more relevant.
- The parameters are proportional to $g_k = \frac{\Omega^2}{Q_k^2} \propto \frac{1}{r^4 Q_k^2}$, given by the directional correlation function $K(\vartheta)$ (see [2]). For the photopeak at 1.5MeV, the ratios are given in Table 1.1. We see that a bigger distance has a bigger effect on the expected count rate than the uncertainty in the angles. So the best choice for this scenario is to choose the detectors to be 5cm away from the source.

r/cm	g_2	g_4
5	1.95	3.16
7	0.47	0.62
10	0.11	0.12

Table 1.1.: Effects on the coincidence count rate at different distances

1.4.2. Which angles to pick?

From [2] we expect $f(\theta) = 1 + 0.1020P_2(\cos\theta) + 0.0091P_4(\cos\theta)$, leading to $A = 0.9524$, $B = \frac{1}{8}$ and $C = \frac{1}{24}$ for $f(\theta) = A \cdot (1 + B\cos^2\theta + C\cos^4\theta)$. Introducing $\alpha = B + C = \frac{1}{6}$ and $\beta = B - C = \frac{1}{12}$ leads to $f(\theta) = A \cdot (1 + \frac{\alpha+\beta}{2}\cos^2\theta + \frac{\alpha-\beta}{2}\cos^4\theta)$. This is plotted, also for varying α and β, in Fig. 1.4. Varying α mostly varies the amplitude surrounding $\theta = 0°, 180°, 360°$, whereas varying β mostly varies the width of the curve, leading to the biggest change at $n \cdot 90° + 45°$. Therefore the region between 120° and 240° is the most sensitive regarding the parameters.
That is why we take the measurements at 135°, 180° and 225° the longest. To be able to get an accurate result for the 'base amplitude' we also carry out long measurements at 90° and 270°. The other measurements we make are shorter, and therefore have a larger relative error.

1.4.3. Correcting for de-adjustment

Ideally, both detectors have the same distance r from the source. In reality, however, the source is not always perfectly in the circle of the setup. So the rate at the movable detector varies as $N_2(\theta) \sim \frac{1}{r_2^2(\theta)}$, and the dependence of the correlation goes as $N_1N_2(\theta) \sim \frac{1}{r^2 r_2^2(\theta)}$ instead of $N^2 \sim \frac{1}{r^4}$. The rate at the fixed detector N_1 is fixed because we do not move this detector. This gives an extra angular dependence in the data of the correlation, beyond what we are expecting from the angular correlation. This can be corrected by assuming the rate in the movable detector should behave the same as in the fixed detector, and multiplying both the rate at the mobile detector and the coincidence rate by the correction factor $k(\theta) = \frac{N_1}{N_2(\theta)}$.

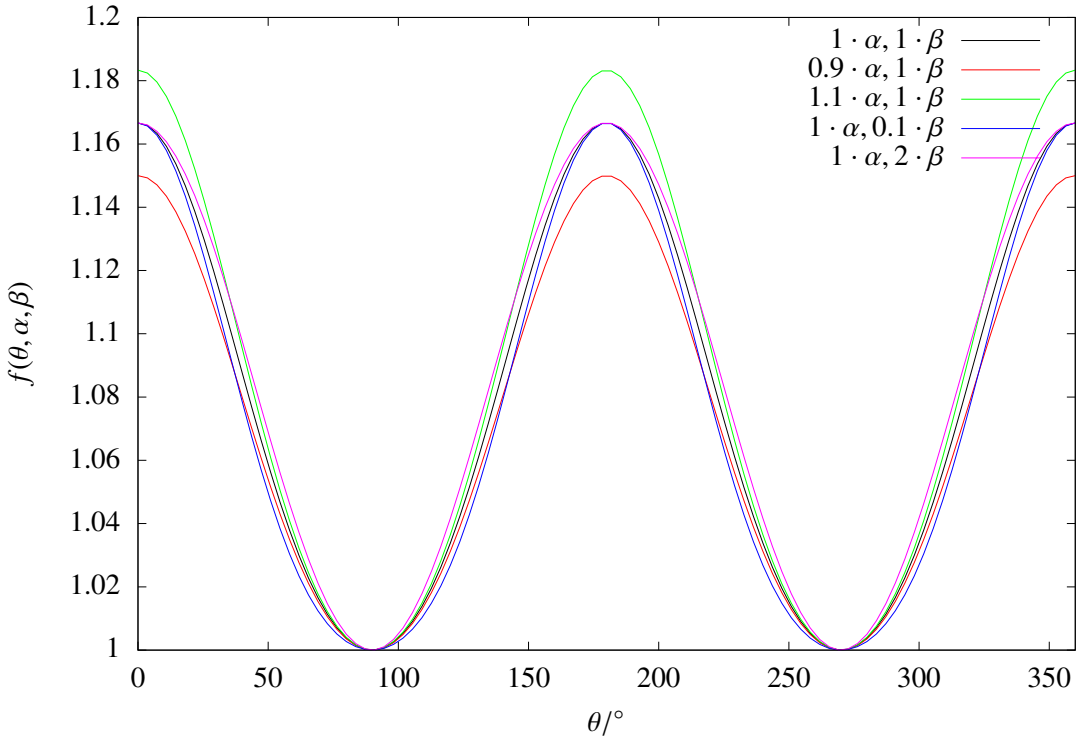

Figure 1.4.: Coincidence function f with varying parameters α and β

2. Analysis of the Data

We are measuring the count rates in a nuclear decay, so we can assume the data follows a Poisson-distribution and thus the error for a count rate N is $\sqrt{N}$, as elaborated in [3]. When we fit a function to our data, we use gnuplot, which internally uses the nonlinear least-squares Marquardt-Levenberg algorithm [4].

2.1. Calibration Measurements

2.1.1. Main Amplifier Gain

The output of the amplifiers are shown in Figs. 2.1 and 2.2. Both show a spectrum with a lot of lines, but they are centered around two distinct points, marked by the solid and dotted lines. They ratio between the height of these pulses is 1.15 ± 0.09 for the fixed detector and 1.13 ± 0.09 for the mobile detector. This fits very well to the ratio 1.14 we are expecting, which is the ratio between the energies of the photopeaks.

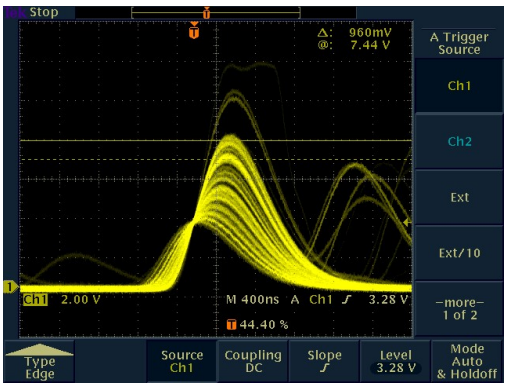

Figure 2.1.: Output of the amplifier of the fixed detector

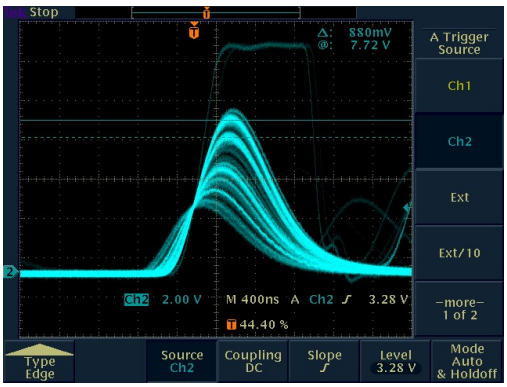

Figure 2.2.: Output of the amplifier of the mobile detector

The signal shape is exactly how we expect it to be from the unipolar output, it is rising fast and falling a little slower after the peak. All signals cross at the triggering point.
If the signals were saturated, they would form a plateau at their maximum. A hint of such a saturated signal can be seen in Fig. 2.2, however, the photopeaks are in a region where the gain is not big enough to saturate the signal.

2.1.2. Calibration of the SCAs

For measuring the spectrum of the detectors, we used the SCA in window mode with a window size of 20 and swept the entire possible region, i. e. between 0 and 1000, for a duration of 5s at each datapoint. The results are plotted in Fig. 2.3 and Fig. 2.4.
For both detectors, we chose windows which cover both photopeaks. This has the advantage that is does not matter which detector detects the first photon of the cascade and which detector the second one, so the count rate for the coincidence is about double as high as if each detector only detected one photopeak. The disadvantage is that the correction factors for the coincidence function are not as exact as they could be, however, the variation is only in the second significant digit.
We deliberately chose the windows on the bigger side, so we have a bit of wiggle room in case there is a bit of a drift in the measuring electronics. For the fixed detector, we chose the window between 560 and 800 scale parts, for the mobile detector we put the boundaries at 580 and 820. These boundaries are also marked in the plots.
To do a cross-check if our windows are reasonable, we connected the output of the SCAs to the oscilloscope. For the mobile detector, the signal of the bipolar output is shown in Fig. 2.5, the output of the fixed detector looks qualitatively the same. As expected, the signal again shows two centers. Here the ratio of the peaks is 1.19 ± 0.15, again corresponding to the ratio between the photopeaks.
So we can conclude that we chose our thresholds for the SCA reasonably, and can continue.

2.1.3. Finding the CFD Threshold

Similar to the measurements for the SCA, we sought for a threshold for the CFD to cancel the contributions from noise to the measurements. Here we also varied the threshold over a big range and measured for 5s for each data point. The results are plotted in Figs. 2.6 and 2.7.
The measurements that were made without the source are pure noise, so we look for a threshold where this signal is small, but we do not have a lot of loss for the signal with the source installed, which is mostly correct measurements. For both detectors we picked a threshold where the noise has dropped by about one order of magnitude, for the fixed detector this is at 50 and for the mobile detector this is at 70. The chosen thresholds are also marked in the plots.
We once again did a cross-check of the signal with the oscilloscope, the signal is shown in Fig. 2.8 for the fixed detector and looks qualitatively identical for the mobile detector. Because the input of the CFD has not been put through the SCA, we again see a very broad spectrum, however, we can see two centers with a ratio of 1.14 ± 0.16, corresponding to the photopeaks.
We see that the CFD is working correctly because the lower boundary of the signal is quite sharp, and changes when we change the CFD-setting.

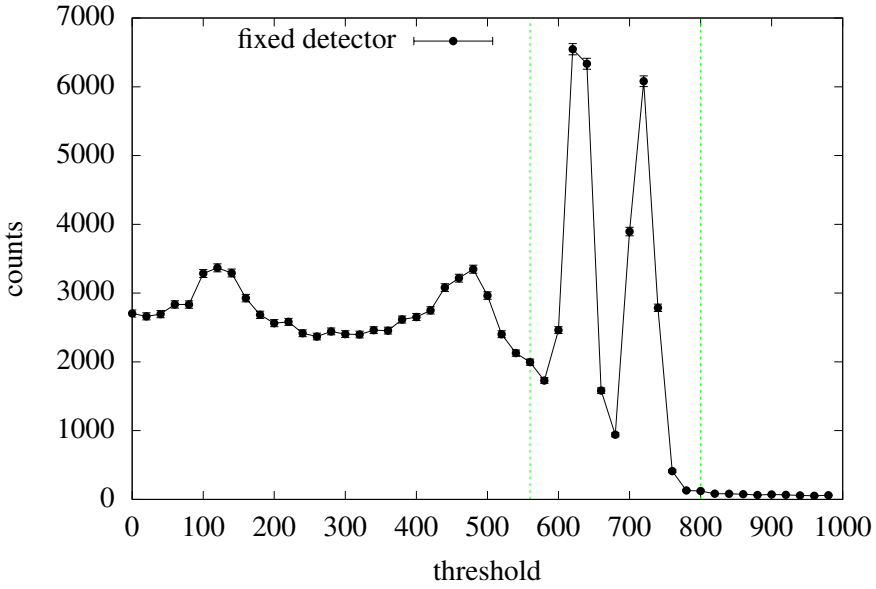

Figure 2.3.: Spectrum of the fixed detector

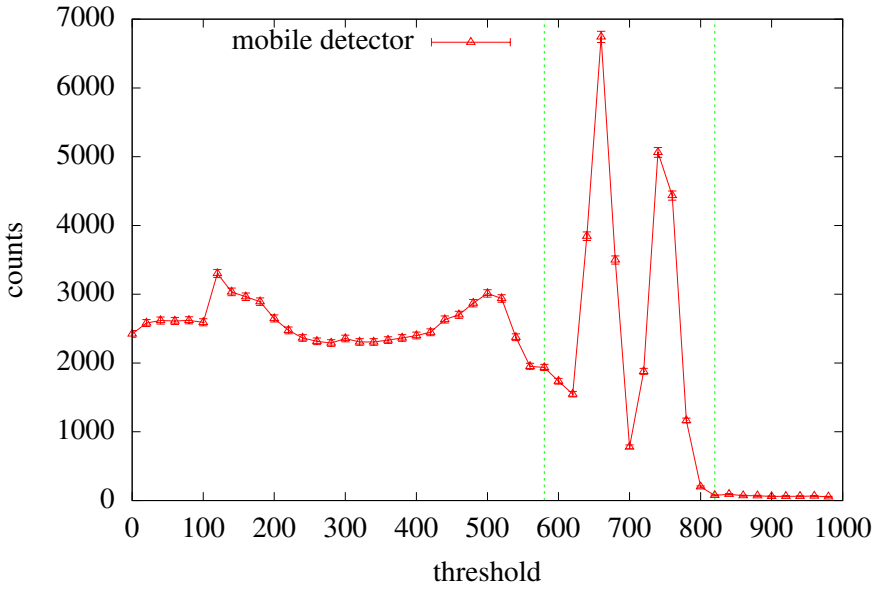

Figure 2.4.: Spectrum of the mobile detector

Figure 2.5.: Bipolar output of the SCA of the mobile detector after setting the thresholds

2.1.4. Delay Adjustment in the Fast Branch

We adjusted the variable delay in the fast circuit in steps of 2ns, the fixed delay is set to 50ns. Again, we measured 5s for each data point. To determine the resolving time, we fit the function

$$f(t) = \frac{A}{2} \cdot \left(1 + \mathrm{erf}\left(\frac{(t - t_0) + \frac{w}{2}}{\sigma}\right) \cdot \mathrm{erf}\left(\frac{-(t - t_0) + \frac{w}{2}}{\sigma}\right)\right) + A_0$$

to the data. The measurement as well as the fit is plotted in Fig. 2.9.
The parameters for the fit are listed in Table 2.1.

	value	error	meaning
A	1159	24	amplitude
A_0	63.1	4.0	constant background
t_0	44.93	0.13	value for the variable delay with which the highest coincidence is recorded
w	29.41	0.41	width of the plateau
σ	5.53	0.30	steepness of the curve
χ^2_{red}	3.39	-	goodness of fit

Table 2.1.: Fit parameters for the delay function

The parameters we are the most interested in are w, which is the resolving time, as well as t_0, which is the delay we have to set for the signals that were detected at the same time to be registered as a coincidence. The other parameters do not have a physical relevance in this experiment. We determine the resolving time to be (29.41 ± 0.41)ns, and the delay as (44.93 ± 0.13)ns. This justifies the value 46ns of the delay that we have chosen to use for the following measurements. This value was chosen by looking at a preliminary plot of the data. The χ^2_{red} value indicates the fit was not ideal, but looking at the graphical representation, all the points follow the expected distribution well.

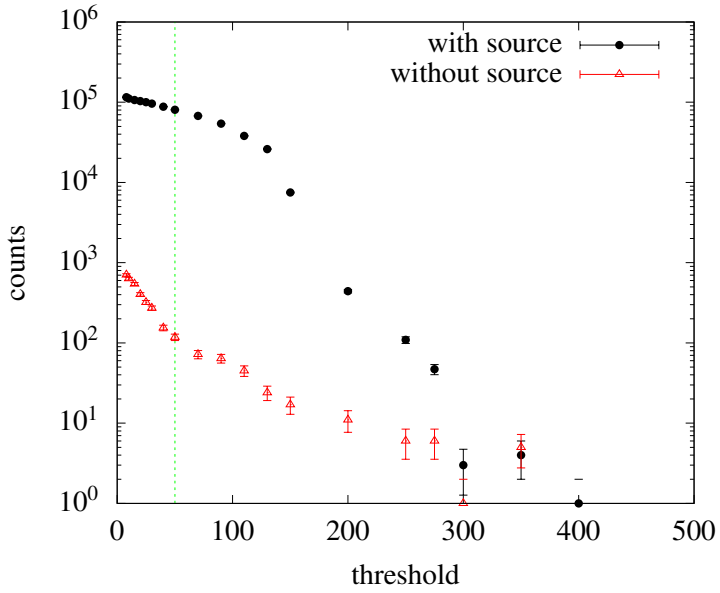

Figure 2.6.: Output of the CFD of the fixed detector

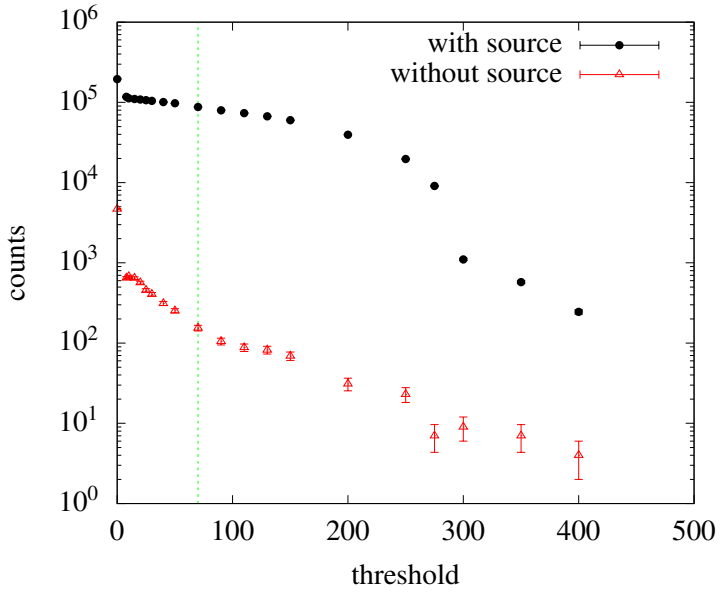

Figure 2.7.: Output of the CFD of the mobile detector

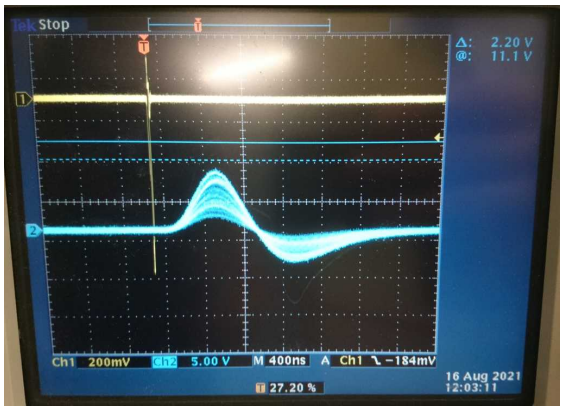

Figure 2.8.: Bipolar output of the CFD of the fixed detector after setting the thresholds

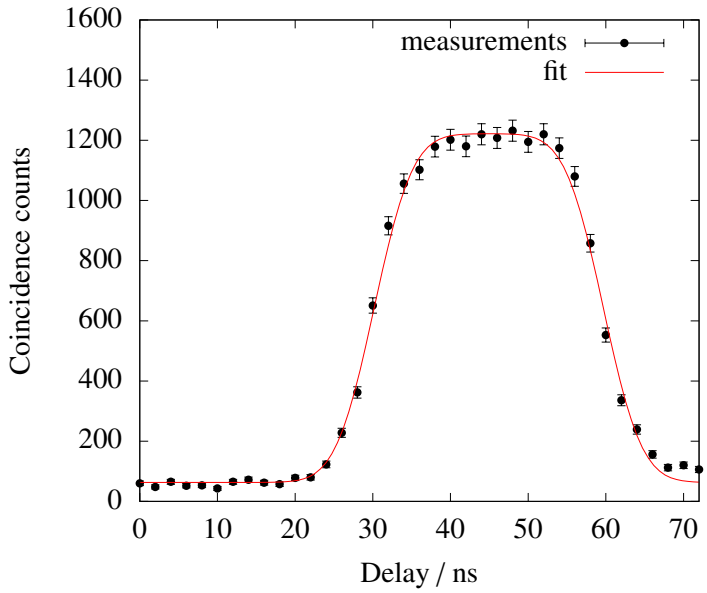

Figure 2.9.: Output of the coincidence module in the fast circuit

The resolving time is long enough so we have a real overlap between the pulses and see a plateau forming. If it were too short, we would only see a spike, and if it were too long, we would run the risk of completely unrelated signals being taken as coincident, or even a constant firing.

2.1.5. Delay Adjustment in the Slow Branch

When setting up the triple coincidence, we aligned the signal from the fast circuit with each signal from the slow circuit. The aligned signals are shown in Figs. 2.10 and 2.11.

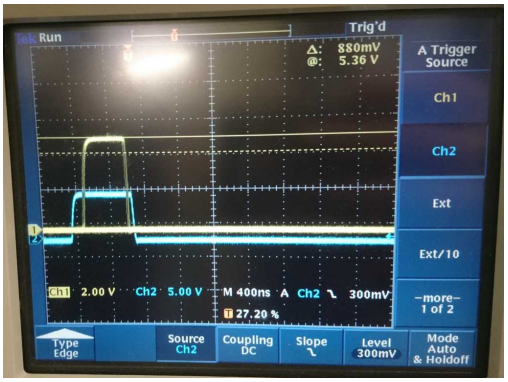

Figure 2.10.: Coincidence of the fast circuit and of the slow circuit of the mobile detector

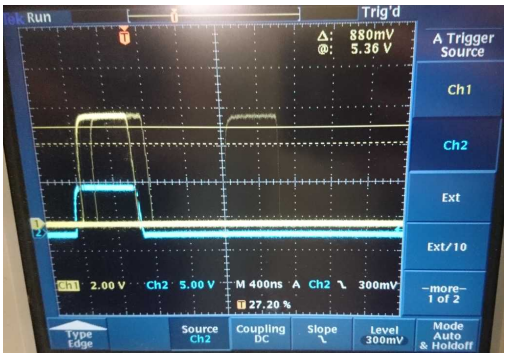

Figure 2.11.: Coincidence of the fast circuit and of the slow circuit of the fixed detector

We used the signal from the fast circuit as the trigger, because this ensures both detectors registered an event at the same time. The slow circuit is then the confirmation that there was indeed a photon of the correct energy detected. The signals overlap in the center to get the longest possible coincidence signal.

2.2. Main Measurement

After the preparation of the electronic setup the main measurement could be taken. Regarding the results of the prepatory tasks it is important to count the coincidences for angles ϑ in the range $90° \ldots 270°$. Especially to determine later the coefficients A_{22} and A_{44} the measurements at 135°, 180° and 225° need to be carried out with high precision. This means that one has to measure for a long time, but this may lead to systematic errors because of drifts in the electronics over time. In order to minimize the effect on the results we made short measurements of 300s or 400s for each angle and repeated the procedure after arriving at the last angle. The idea is that all angles are equally affected by the drifting and the error cancels out. The angles we picked can be found, together with the measuring times we used and the number of measurements, in Table 2.2.

ϑ / °	time total / s	# of meas.
90	1000	3
110	300	1
120	300	1
135	1000	3
150	300	1
160	700	2
180	1000	3
200	700	2
210	300	1
225	1000	3
240	300	1
250	300	1
270	1000	3

Table 2.2.: Overview of angles, measuring times and number of measurements

2.2.1. Stability and Corrections of the Measurement

First, we check the stability of our setup by looking at the temporal evolution of the count rate of the fixed detector depicted in Fig. 2.12. One observes in fact a slight decrease of the count rate by fitting a linear function $f(x) = mx + n$ to the data, but each rate lays within the first standard deviation of the other data points. Therefore, the tiny $\chi^2_{\text{red}} = 0.04$ indicates an overfitting. Also the resulting values of the fit parameters and the high relative error of the slope m stress the uncertainty and smallness of the decrease:

$$m = (-0.006 \pm 0.003)\frac{1}{\text{s}}, \quad n = (66.26 \pm 0.04)\frac{1}{\text{s}}$$

Because of that and the repeated measurements we made for the most important angles we decided to neglect the drift of the fixed detector.
Similarly, the count rates N_2 of the mobile detector at a given angle have overlapping error regions as seen in Fig. 2.13. The angle-dependent change of the count rates may be explained by a misalignment of the setup. As we took repeated measurements for several angles we can compare the evolution of the coincidence count rate C for a fixed angle. However, there is no clear drift remarkable in the data shown in Fig. 2.14. There is a small decrease in the count rate for 90°, 160°, 200° and 270° and a fluctuating behaviour for 135°, 180° and 225°. The errorbars of the data are too short to be visible. In conclusion there are instabilities but no specific drift observable. For a further examination of the stability more repetitions of the measurements may have helped.
In the following we ignore the slight instability because we have seen for the fixed and mobile detector that the drift lays within the standard deviation and the data from the coincidence count rate does not present any significant trend.
Next, the experimental data of the counted coincidences need to be corrected for accidental coincidences that may be caused by events of two nuclei decaying simultaneously and are not

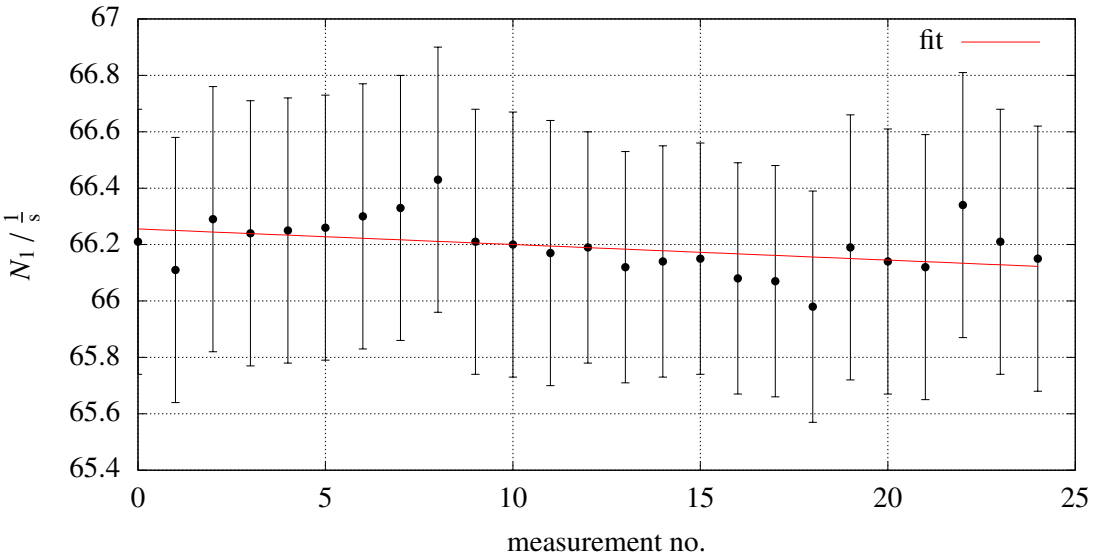

Figure 2.12.: Count rate N_1 of the fixed detector against the measurement

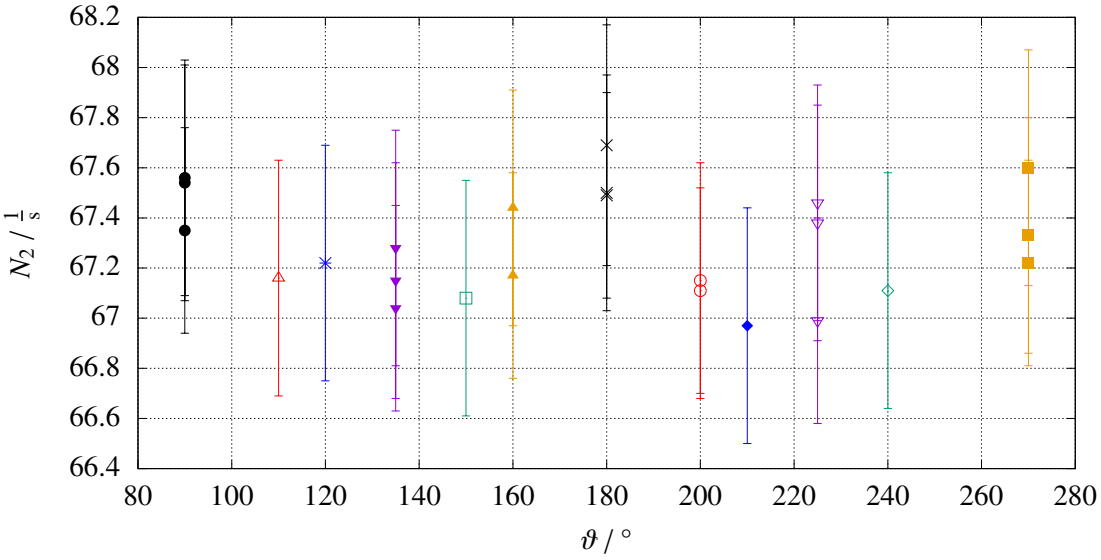

Figure 2.13.: Count rate N_2 of the mobile detector for given angles ϑ

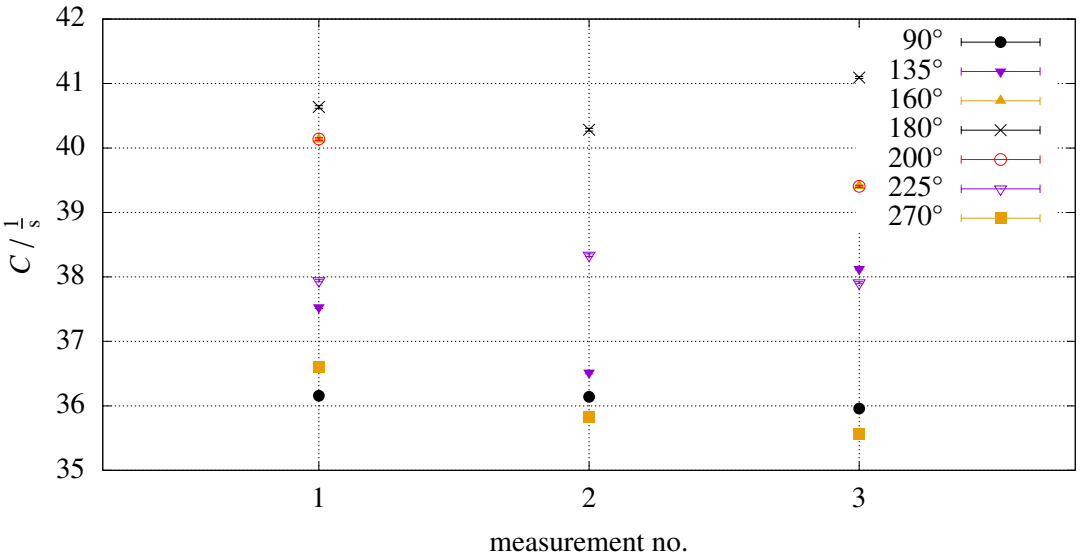

Figure 2.14.: Coincidence count rate C against the measurement at a fixed angle ϑ

due to a γ–γ cascade. Consequently, the two γ-rays are uncorrelated and one expects an isotropic distribution of the random coincidences for all angles.
Using the resolving time w determined in section 2.1.4 the rate of accidental coincidences C_{acc} is found by $C_{\text{acc}} = 2wN_1N_2$ [2]. For our measurements this yields a variance-weighted mean rate $C_{\text{acc}}^{\text{theo}} = (2.63 \pm 0.02) \cdot 10^{-4} \frac{1}{\text{s}}$. In contrast to this result, the accidental count rate from the direct measurement by setting the variable delay at the fixed detector to 0ns is with $C_{\text{acc}}^{\text{meas}} = (1.24 \pm 0.03) \frac{1}{\text{s}}$ bigger by four orders of magnitude. Setting the delay to 0ns ensures that we are in a region of the delay where truly coincident signals do not arrive at the same time, so we only see the random coincidences. The high discrepancy between the two rates of C_{acc} could arise from the still remaining electronic noise after applying the CFD threshold because we need to take a compromise between filtering noise and maximizing the count rate. Therefore, we assume that the experimental value is more realistic and correct the measured coincidence count rates by subtracting it.
Another correction has to be considered in case of a misalignment of the setup. If the source is not exactly positioned in the center or the distances of the scintillation detectors is not equal towards the source, this has an effect on the measured count rates. In an ideal setup the count rates of the fixed and the mobile detector are equal, however, this is not the case in the real setup. To compensate the misalignment we calculate for each angle the ratio $k(\vartheta) = N_1/N_2(\vartheta)$ between the count rate N_1 of the fixed detector and the count rate N_2 of the mobile detector to find the correction factor $k(\vartheta)$ for $N_2^{\text{corr}} = k(\vartheta)N_2$. Subsequently, we multiply the coincidence count rate by this factor because $C(\vartheta) \propto N_1N_2^{\text{corr}} = k(\vartheta) \cdot N_1N_2$. The correction factors $k(\vartheta)$ are given in Table A.1, the final corrected count rates in Table A.2 in the appendix.

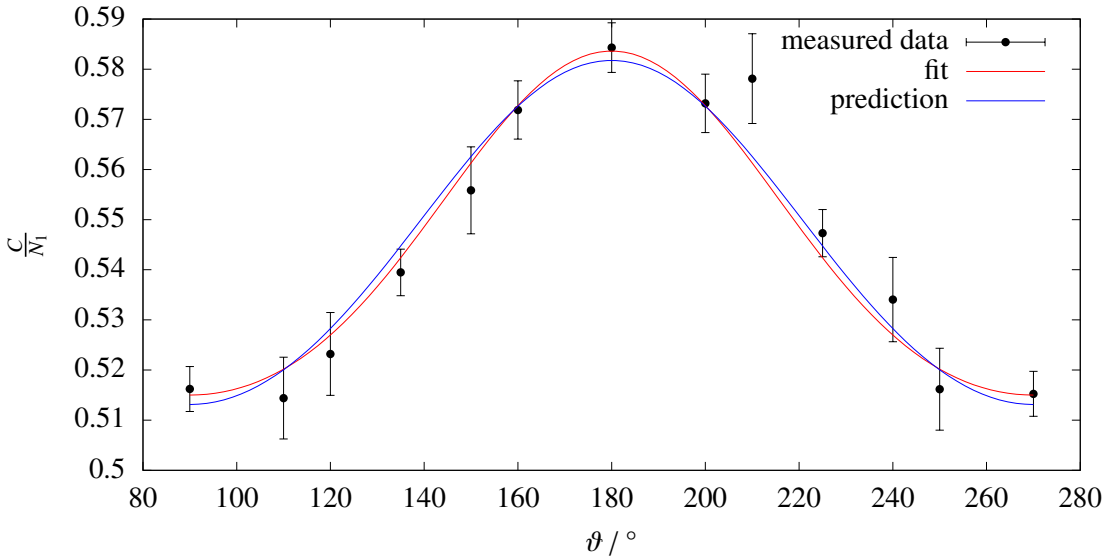

Figure 2.15.: Data, fit and prediction of the γ–γ angular correlation. The data point of $\vartheta = 210°$ was excluded from the fit.

2.2.2. Analysis of the Angular Distribution

Finally, the coincidence rates are corrected and can be used to investigate the directional correlation of the γ–γ cascade. As the directional correlation function $K(\vartheta)$ is proportional to $C/N_1 =: \widetilde{K}(\vartheta)$ [2] we determine the ratio between the corrected coincidence count rate and the count rate of the fixed detector. The data is plotted in Fig. 2.15 with a fit of the function

$$K(\vartheta) \propto \widetilde{K}(\vartheta) = \widetilde{K}_0 \cdot \left[\left(1 - \frac{1}{2}A_{22} + \frac{3}{8}A_{44}\right) + \left(\frac{3}{2}A_{22} - \frac{15}{4}A_{44}\right)\cos^2\vartheta + \left(\frac{35}{8}A_{44}\right)\cos^4\vartheta\right]$$

which follows from the formula $K(\vartheta) = K_0 \cdot [1 + A_{22}P_2(\cos\vartheta) + A_{44}P_4(\cos\vartheta)]$ in [2]. The values for $\widetilde{K}(\vartheta)$ are also given in Table A.3 in the appendix.
In the fit we have omitted the measurement of $\vartheta = 210°$ because it is the only data point which is far off the expected curve and it belongs to the angles that were not measured for a long period of time. This is why its accuracy is questionable, however, we did not do an additional measurement of this angle at the lab to confirm the doubt due to the late recognition of the deviation.
The experimental data is not measured for infinitesimal solid angles due to the spatial extension of the scintillation crystal and therefore it is necessary to apply correction factors Q_k to the found parameters A_{22}^{exp} and A_{44}^{exp} to obtain the true coefficients $A_{kk} = A_{kk}^{\text{exp}}/Q_k^2$. The corresponding correction factors $Q_2 = 0.9057$ and $Q_4 = 0.7114$ for our setup are taken from [2], as shown in Fig. A.1, for a $2'' \times 2''$ crystal at a distance of 5cm from the radioactive source. The calculated fit parameters and the corrected coefficients A_{kk} are summarized in Table 2.3. The χ^2_{red} value of the fit is 0.407, indicating that the datapoints follow the expected distribution very closely.

$\widetilde{K}_0$	A_{22}^{exp}	A_{44}^{exp}	A_{22}	A_{44}
0.546 ± 0.001	0.113 ± 0.006	0.013 ± 0.004	0.138 ± 0.008	0.03 ± 0.01

Table 2.3.: Results of the fit and correction for the angular correlation

By theoretical calculation [2] one finds the values

$$A_{22}^{\text{theo}} = 0.1020, \quad A_{44}^{\text{theo}} = 0.0091$$

that are approximately in the same order of magnitude as the measured coefficients, but do not lay within their 1σ-regions. For both coefficients we observe that the measured value is greater than the theoretical one.
The prediction drawn in blue in Fig. 2.15 was determined by fitting the theoretically expected function

$$\widetilde{K}^{(420)}(\vartheta) = \widetilde{K}_0^{(420)} \cdot \left[1 + A_{22}^{\text{theo}} Q_2^2 P_2(\cos\vartheta) + A_{44}^{\text{theo}} Q_4^2 P_4(\cos\vartheta)\right]$$

via the scaling factor $\widetilde{K}_0^{(420)}$ to the measured data. The data follow the predicted function within the statistical expectation.
Comparing data, fit and prediction we can try to explain the reasons of the deviations. First of all, one remarks that the data points for $90° < \vartheta < 180°$ are all below the fit and the prediction function which hints to a remaining misalignment of the source despite the correction in subsection 2.2.1. Perhaps this is caused by a de-adjustment of the platform of the mobile detector. In addition to this the residual electronic noise leads to a scattering of the data.
For the fit and prediction of the angular distribution a 4-2-0 cascade of the nuclear spin has been assumed. By fitting some other known distribution functions of different cascades to the measured data depicted in Fig. 2.16 one can easily exclude the other cascades as they do not match the observations. The distribution functions from [2] for a 0-1-0, a $\frac{1}{2}$-$\frac{1}{2}$-$\frac{1}{2}$ and $\frac{1}{2}$-$\frac{3}{2}$-$\frac{1}{2}$ cascade have been compared to the measurement:

$$\begin{aligned}
\widetilde{K}^{(010)}(\vartheta) &= \widetilde{K}_0^{(010)} \cdot \left[1 + \tfrac{1}{2} Q_2^2 P_2(\cos\vartheta)\right] \\
\widetilde{K}^{(\frac{1}{2}\frac{1}{2}\frac{1}{2})}(\vartheta) &= \widetilde{K}_0^{(\frac{1}{2}\frac{1}{2}\frac{1}{2})} \\
\widetilde{K}^{(\frac{1}{2}\frac{3}{2}\frac{1}{2})}(\vartheta) &= \widetilde{K}_0^{(\frac{1}{2}\frac{3}{2}\frac{1}{2})} \cdot \left[1 + \tfrac{1}{4} Q_2^2 P_2(\cos\vartheta)\right]
\end{aligned}$$

which gives rise to the scaling factors

$$\begin{aligned}
\widetilde{K}_0^{(010)} &= 1.2 \pm 0.3 \\
\widetilde{K}_0^{(\frac{1}{2}\frac{1}{2}\frac{1}{2})} &= 0.542 \pm 0.008 \\
\widetilde{K}_0^{(\frac{1}{2}\frac{3}{2}\frac{1}{2})} &= 0.52 \pm 0.01
\end{aligned}$$

Given the precise measurements at 90°, 160°, 180°, 200° and 270° the mismatch to the other cascades is higher than 3σ while the experimental data are in harmony with the curve of the

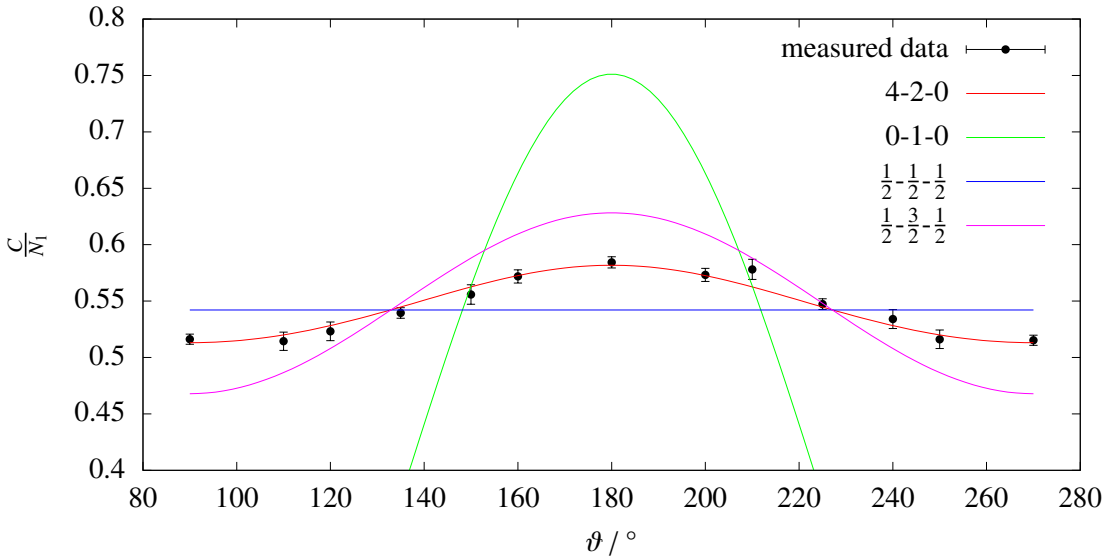

Figure 2.16.: Fits of cascades with different spins to the measured data

4-2-0 cascade. As before we excluded the data point $\vartheta = 210°$ from the fits. A sudden increase at 210° is expected for neither of the cascades and since it is a single data point with a relatively high error compared to the above more precise ones, it does not yield a sufficient significance and may be neglected.
Another indicator that the curve of the 4-2-0 cascade suits our data the best is the χ^2_{red} value of the fits. For the 0-1-0, the $\frac{1}{2}$-$\frac{1}{2}$-$\frac{1}{2}$ and the $\frac{1}{2}$-$\frac{3}{2}$-$\frac{1}{2}$ cascade its value equals 3593, 20.8 and 40.3 respectively, which hints to a poor fitting model. In contrast to them, the fit of the 4-2-0 cascade has a $\chi^2_{\text{red}} = 0.431$ which is already a sign of a fit that is 'too good'.

Conclusion

The setup was done reasonably, as evidenced by the cross-checks with the oscilloscopes, and the agreement of our observed curves with the expectations. Especially the variable delay that was chosen by only a brief look at the data is in very nice agreement with the one determined by the fits.
There are some instabilities in the data, especially the slightly decreasing count rate, however, these effects are small and we did not do any adjustments for the decreasing count rate. We adjusted the data for an asymmetric setup.
The fit of our data to a 4-2-0 cascade resulted in parameters that were in the same order of magnitude as the expected ones, but the disagreement was about 3σ. However, our data also follow the theoretical prediction very nicely. Doing a fit to other conceivable cascades showed these do not describe our data well at all.
The measurements might be improved by a more thorough analysis of the instabilities in the data, and also by longer measuring times.
In conclusion, our measurements confirmed that a 4-2-0 cascade is the best description of the γ-rays emitted by ^{60}Co.

A. Appendix

$\vartheta/^\circ$	n_1	n_2	$k(\vartheta) = n_1/n_2$	$\sigma(k(\vartheta))$
90	66237	67472	0.982	0.005
110	19857	20147	0.986	0.010
120	19835	20167	0.984	0.010
135	66210	67145	0.986	0.005
150	19903	20124	0.989	0.010
160	46342	47099	0.984	0.006
180	66196	67553	0.980	0.005
200	46308	46991	0.985	0.006
210	19864	20092	0.989	0.010
225	66166	67251	0.984	0.005
240	19846	20134	0.986	0.010
250	19841	20202	0.982	0.010
270	66132	67368	0.982	0.005

Table A.1.: Correction factors $k(\vartheta)$ for the misalignment using the total count rates n_1 and n_2 of the detectors

TABLE 3

Correction factors for 2″ × 2″ crystals.
Calculated by E. Matthias using the present programme

h (cm)	E (MeV)	ε		Q_2		Q_4	
		Whole spectrum	Photopeak	Whole spectrum	Photopeak	Whole spectrum	Photopeak
10.0	1.5	0.4163	0.1108	0.9657	0.9692	0.8888	0.8999
	1.0	0.4781	0.1648	0.9653	0.9686	0.8876	0.8979
	0.7	0.5417	0.2449	0.9649	0.9678	0.8861	0.8955
	0.5	0.6116	0.3539	0.9642	0.9671	0.8842	0.8933
	0.3	0.7523	0.6167	0.9624	0.9643	0.8785	0.8845
	0.2	0.8640	0.8103	0.9597	0.9607	0.8700	0.8732
	0.15	–	–	0.9576	0.9576	0.8635	0.8646
	0.10	0.9694	0.9603	0.9557	0.9557	0.8573	0.8575
	0.05	0.9950	0.9933	0.9545	0.9545	0.8538	0.8538
	0.03	0.9907	0.9869	0.9547	0.9547	0.8544	0.8544
	0.02	0.9971	0.9958	0.9544	0.9544	0.8535	0.8535
7.0	1.5	0.3796	0.0993	0.9378	0.9440	0.8032	0.8222
	1.0	0.4375	0.1485	0.9369	0.9441	0.8006	0.8225
	0.7	0.4976	0.2202	0.9359	0.9422	0.7976	0.8167
	0.5	0.5648	0.3265	0.9346	0.9403	0.7935	0.8109
	0.3	0.7055	0.5736	0.9306	0.9345	0.7815	0.7932
	0.2	0.8288	0.7757	0.9246	0.9265	0.7636	0.7694
	0.10	0.9599	0.9507	0.9152	0.9153	0.7358	0.7363
	0.05	0.9934	0.9917	0.9124	0.9124	0.7278	0.7278
	0.03	0.9877	0.9839	0.9129	0.9129	0.7292	0.7293
	0.02	0.9961	0.9948	0.9122	0.9122	0.7272	0.7272
5.0	1.5	0.3472	0.0925	0.8947	0.9057	0.6801	0.7114
	1.0	0.4014	0.1421	0.8930	0.9046	0.6754	0.7086
	0.7	0.4584	0.2017	0.8911	0.9016	0.6699	0.7001
	0.5	0.5230	0.3007	0.8885	0.8981	0.6626	0.6901
	0.3	0.6633	0.5366	0.8808	0.8879	0.6411	0.6612
	0.2	0.7963	0.7439	0.8693	0.8727	0.6094	0.6188
	0.10	0.9510	0.9419	0.8503	0.8505	0.5587	0.5593
	0.05	0.9919	0.9902	0.8444	0.8444	0.5436	0.5436
	0.03	0.9850	0.9813	0.8455	0.8455	0.5462	0.5463
	0.02	0.9952	0.9939	0.8439	0.8439	0.5423	0.5424

Figure A.1.: Solid angle correction factors (extracted from [2])

experimental data				$C' = C - C_{\text{acc}}$		$C^{\text{corr}} = k(\vartheta) \cdot C'$	
$\vartheta/^\circ$	duration / s	$C/\frac{1}{\text{s}}$	$\sigma(C)/\frac{1}{\text{s}}$	$C'/\frac{1}{\text{s}}$	$\sigma(C')/\frac{1}{\text{s}}$	$C^{\text{corr}}/\frac{1}{\text{s}}$	$\sigma(C^{\text{corr}})/\frac{1}{\text{s}}$
90	1000	36.07	0.19	34.83	0.19	34.19	0.27
110	300	35.79	0.35	34.55	0.35	34.05	0.48
120	300	36.41	0.35	35.17	0.35	34.59	0.49
135	1000	37.46	0.19	36.22	0.20	35.72	0.27
150	300	38.53	0.36	37.29	0.36	36.88	0.51
160	700	39.72	0.24	38.48	0.24	37.86	0.34
180	1000	40.71	0.20	39.47	0.20	38.68	0.29
200	700	39.72	0.24	38.48	0.24	37.92	0.34
210	300	39.96	0.36	38.72	0.37	38.28	0.53
225	1000	38.05	0.20	36.81	0.20	36.21	0.28
240	300	37.08	0.35	35.84	0.35	35.33	0.50
250	300	36.00	0.35	34.76	0.35	34.14	0.48
270	1000	35.95	0.19	34.71	0.19	34.07	0.27

Table A.2.: Correction of the count rates of coincidences for accidental coincidences and misalignment of the setup.

$\vartheta/^\circ$	$\widetilde{K}(\vartheta)$	$\sigma(\widetilde{K}(\vartheta))$
90	0.516	0.004
110	0.514	0.008
120	0.523	0.008
135	0.539	0.005
150	0.556	0.009
160	0.572	0.006
180	0.584	0.005
200	0.573	0.006
210	0.578	0.009
225	0.547	0.005
240	0.534	0.008
250	0.516	0.008
270	0.515	0.004

Table A.3.: Data of the angular distribution function $\widetilde{K}(\vartheta)$

List of Figures

List of Tables

Bibliography

[1] *K223: Nuclear γ–γ Angular Correlations*. manual provided by the tutor. July 2021.

[2] Kai Siegbahn, ed. *Alpha-, beta- and gamma-ray spectroscopy. 2*. 5. print. Amsterdam u.a.: North-Holland [u.a.], 1979. ISBN: 9780720400830.

[3] William R. Leo. *Techniques for Nuclear and Particle Physics Experiments*. 1994. ISBN: 3-540-57280-5.

[4] Thomas Williams and Colin Kelley. *gnuplot 5.2 - an interactive plotting program*. last checked 24.08.2021. URL: `http://gnuplot.sourceforge.net/docs_5.2/Gnuplot_5.2.pdf`.